REPORT DOCUMENTATION PAGE	Form Approved OMB No. 0704-0188

1. AGENCY USE ONLY *(Leave blank)*	2. REPORT DATE	3. REPORT TYPE AND DATES COVERED
	28.Oct.03	MAJOR REPORT

4. TITLE AND SUBTITLE
"CONFOCAL MICROSCOPY FOR REAL-TIME DETECTION OF ORAL CAVITY NEOPLASIA"

5. FUNDING NUMBERS

6. AUTHOR(S)
MAJ CLARK ANNE L

7. PERFORMING ORGANIZATION NAME(S) AND ADDRESS(ES)
UNIVERSITY OF TEXAS AT AUSTIN

8. PERFORMING ORGANIZATION REPORT NUMBER
CI02-1298

9. SPONSORING/MONITORING AGENCY NAME(S) AND ADDRESS(ES)
THE DEPARTMENT OF THE AIR FORCE
AFIT/CIA, BLDG 125
2950 P STREET
WPAFB OH 45433

10. SPONSORING/MONITORING AGENCY REPORT NUMBER

11. SUPPLEMENTARY NOTES

12a. DISTRIBUTION AVAILABILITY STATEMENT
Unlimited distribution
In Accordance With AFI 35-205/AFIT Sup

DISTRIBUTION STATEMENT A
Approved for Public Release
Distribution Unlimited

12b. DISTRIBUTION CODE

13. ABSTRACT *(Maximum 200 words)*

20031104 024

14. SUBJECT TERMS

15. NUMBER OF PAGES
37

16. PRICE CODE

17. SECURITY CLASSIFICATION OF REPORT	18. SECURITY CLASSIFICATION OF THIS PAGE	19. SECURITY CLASSIFICATION OF ABSTRACT	20. LIMITATION OF ABSTRACT

THE VIEWS EXPRESSED IN THIS ARTICLE ARE THOSE OF THE AUTHOR AND DO NOT REFLECT THE OFFICIAL POLICY OR POSITION OF THE UNITED STATES AIR FORCE, DEPARTMENT OF DEFENSE, OR THE U.S. GOVERNMENT

Confocal Microscopy for Real Time Detection of Oral Cavity Neoplasia

A. L. Clark[1], A. Gillenwater[2], T. Collier[1], R. Alizadeh-Naderi[2], A. K. El-Naggar[2],

R. Richards-Kortum[1]

[1]Department of Biomedical Engineering, University of Texas at Austin, TX, USA

[2]Departments of Head and Neck Surgery and Pathology, The University of Texas M.D.

Anderson Cancer Center, Houston, TX, USA

Research Support

This research was supported by the National Institutes of Health (Grant #1 RO1 CA

82880-01).

Corresponding Author

Dr. Rebecca Richards-Kortum

Department of Biomedical Engineering

The University of Texas at Austin

1 University Station C0800

Austin, Texas 78712

Work: (512) 471 – 2104

Fax: (512) 475 – 8854

E-mail: kortum@mail.utexas.edu

Running Title: Confocal Microscopy for Detecting Oral Neoplasia

Keywords: Optical imaging, Dysplasia, Amelanotic tissue, Squamous cell carcinoma

Abstract

Purpose: The goal of this study was to characterize features of normal and neoplastic oral mucosa using reflectance confocal microscopy.

Experimental Design: Oral cavity biopsies were acquired from 17 patients at the Head and Neck Clinic of the University of Texas M. D. Anderson Cancer Center who were undergoing surgery for squamous cell carcinoma (SCC) within the oral cavity. Reflectance confocal images were obtained at multiple image plane depths from biopsies within six hours of excision. Following imaging, biopsies were fixed in 10% formalin and submitted for routine histologic examination. Reflectance confocal images were compared to histologic images from the same sample to determine which tissue features contribute to image contrast and can be potentially imaged using *in vivo* confocal microscopy.

Results: Confocal images were successfully acquired from 15 biopsy pairs from 17 patients. Depth-related changes in cell diameter and nuclear density were observed at multiple anatomic sites within the oral cavity. In SCCs, densely packed, pleomorphic tumor nuclei could be visualized with distinct differences in nuclear density and morphology distinguishable between confocal images of neoplastic and non-neoplastic oral cavity. Other features of non-cancerous and cancerous oral tissue that could be identified in the confocal images included areas of inflammation, fibrosis, muscle fibers and salivary glands.

Conclusions: Our results support the potential for this tool to play a significant role in the clinical evaluation of oral lesions, real-time identification of tumor margins, and monitoring of response to therapeutic treatment.

Introduction

Confocal reflectance microscopy is a new technology that can provide detailed images of tissue architecture and cellular morphology of living tissue in near real time. In concept, *in vivo* confocal imaging resembles histologic tissue evaluation, except that 3D sub-cellular resolution is achieved non-invasively and without stains. In epithelial structure, resolution of 1 micron has been achieved with a 200-400 micron field of view and a penetration depth of up to 500 microns[1-6]. Recently, flexible reflectance confocal microendoscopes have been described which can obtain high resolution confocal images of tissue *in vivo* in near real time[7-15]. Use of this instrument provides the potential to image oral epithelial tissues with subcellular resolution in a clinical setting.

Confocal imaging with reflected light allows for detailed images of cell morphology and tissue architecture using backscattering by various tissue components to provide contrast. In skin[1, 2, 16-18], cytoplasmic melanin provides a strong source of backscattering, enabling detailed morphologic images of epithelial cell morphology and tissue architecture throughout the entire epithelial thickness. This technology has been used to image various types of skin pathology, including psoriasis[19], folliculitis[20], and neoplastic skin lesions[21-23]. In neoplastic skin lesions, morphologic changes in cytologic structure and microvasculature were visualized in both basal cell carcinomas and melanomas.

In amelanotic epithelial tissues, cell nuclei provide the primary source of reflected light[6, 24] captured by a reflectance confocal microscope. The backscattering from these nuclei is dramatically enhanced by addition of weak (3-6%) acetic acid[25]. Confocal imaging of oral mucosa in the lip and tongue has resolved subcellular detail at depths of

250 microns and 500 microns, respectively[4]. Recent work showed that reflectance confocal imaging of normal and precancerous cervical tissue can characterize nuclear size, nuclear density and nuclear to cytoplasmic ratio without the need for tissue sectioning or staining. Parameters extracted from confocal images could be used to discriminate high grade cervical precancers with a sensitivity of 100% and a specificity of 91% in a study of 25 samples[5]. These results underscore the potential role of this technology in clinical evaluation of oral lesions and the need for further investigations in oral tissue using multiple anatomic sites and pathologic diagnosis.

The goal of this study was to characterize the features of normal and neoplastic oral mucosa using reflectance confocal microscopy. We report results of a pilot study using near real-time reflectance confocal microscopy to image pairs of clinically normal and abnormal biopsies obtained from 17 patients. We find that confocal microscopy can image oral mucosa with resolution comparable to histology without the need for tissue fixation, sectioning or staining. Confocal images provide a detailed view of cell morphology and tissue architecture, demonstrating features of normal epithelium, dysplasia, and squamous carcinoma. Based on these results, we recommend that reflectance confocal microscopy should be explored as a tool to improve early detection of oral cavity neoplasia, to provide real time determination of mucosal tumor margins, and to determine response to therapy.

Methods and Materials

Specimens. Oral cavity biopsies were acquired from 17 patients at the Head and Neck Clinic of the University of Texas M. D. Anderson Cancer Center who were

undergoing surgery for squamous cell carcinoma (SCC) within the oral cavity. Informed consent was given by all patients, and the project was reviewed and approved by the University of Texas M. D. Anderson Cancer Center Office of Protocol Research and the Institutional Review Board at the University of Texas at Austin. Biopsies (approximately 3 mm wide by 4 mm long by 2 mm thick) were acquired from one clinically normal appearing and one clinically suspicious area and immediately placed in growth medium (DMEM, no phenol red). Reflectance confocal images were obtained at multiple image plane depths from biopsies within six hours of excision. Following imaging, biopsies were fixed in 10% formalin and submitted for routine histologic examination by an experienced head and neck pathologist (AEN). Additional sections from each biopsy were stained with Monoclonal Mouse anti-Cytokeratin (Pan) (MMAC) Concentrate Antibody (Zymed Laboratories, Inc.), a broad spectrum monoclonal antibody cocktail of clones A1 and A3 which reacts to cytokeratins 10, 14/15, 16 and 19 in the acidic subfamily and all members of the basic subfamily, to assess correlations between confocal image features and the presence of keratin in the specimen.

Confocal System. Reflectance confocal images were obtained from each biopsy using a near real-time, epi-illumination, reflectance confocal microscope[26] (Fig. 1). Illumination was provided by a continuous wave laser diode operating at 810 nm. A mirror system provided an image frame rate of 7.5 frames per second by scanning illumination light in the sample via a water immersion microscope objective (25X, 0.8 NA). Average illumination power was 10 – 30 mW, focused to a 1 micron-diameter spot on the sample. Light backscattered from the tissue returned to a beam splitter where it

was reflected onto a pinhole lens and then spatially filtered by a 10 μm diameter pinhole aperture before being detected by an avalanche photodiode. The confocal system operated at a dimensionless pinhole radius of 2.5 to provide maximum optical sectioning for obtaining cellular detail[26]. The measured lateral and axial resolution of the system were 0.8 microns and 2-3 microns, respectively. The field of view was adjustable from 300 – 400 microns by changing the system magnification.

Imaging and Image Processing. Prior to imaging, the biopsies were removed from growth media, rinsed with phosphate buffered solution (PBS), and oriented so the image plane of the confocal microscope was parallel to the epithelial surface and would approach the epithelial layer first. A 6% solution of acetic acid was then added to each sample to increase image contrast[25]. Frames were acquired at various epithelial depths until either tissue details were no longer resolvable or up to the working distance of the microscope objective (250 microns). To contrast confocal images obtained in this 'en face' orientation with the traditional radial orientation, additional confocal images were acquired from one biopsy oriented so that the image plane of the confocal microscope was perpendicular to the epithelial surface and from two hundred micron thick transverse organ cultures prepared from biopsies from one patient.

Each of the confocal image frames presented here was resampled and processed to enhance image quality. Resampling was performed to reduce distortion in the images caused by nonlinearity in the resonant galvonometric scanning system while image quality was improved by increasing brightness and contrast within the images. Brightness was enhanced by adding a selected percentage of full gray scale to each pixel

and contrast increased by removing another percentage of full gray scale from the image and expanding the remaining midrange gray levels. Brightness and contrast for all confocal images in this paper were increased by 70% and 50%, respectively. Confocal images from the transverse tissues slices were also tiled together to provide large-scale mosaic views of each slice.

Images of stained histologic sections were acquired using a color CCD camera coupled to a brightfield microscope. Reflectance confocal images were compared to histologic images from the same sample to determine which tissue features contribute to image contrast and can be potentially imaged using *in vivo* confocal microscopy. The confocal microscope's small field of view makes it extremely difficult to register exactly where in the biopsy images were acquired so we identified areas in histologic sections that corresponded to features present in our confocal images.

Results

Images were successfully obtained from specimens from 15 of 17 biopsy pairs with resolution similar to that provided by bright-field microscopy typically used to examine histologic sections; data could not be obtained from two patient specimens due to instrument errors, and these were not included in further analyses. Table 1 shows the number of clinically normal and abnormal specimens obtained from each site within the oral cavity. Table II lists the histopathologic diagnoses for each biopsy from each patient with 15 showing hyperkeratosis or parakeratosis, six exhibiting hyperplasia, one with dysplasia, nine moderately differentiated SCCs, one well differentiated SCC, and three specimens having no diagnosis due to the lack of epithelium in the histologic section.

Figure 2 shows a comparison of histologic (Fig. 2A) and confocal (Fig. 2B) images from the 200 micron thick transverse organ cultures obtained from the normal gingiva biopsy. In the confocal image mosaic, epithelial cell nuclei are apparent throughout the mucosa with the epithelial stromal junction clearly visible (double arrows). In the stroma, connective tissue and fibroblast nuclei (arrow) can be visualized. Figure 2 also shows histologic (Fig. 2C) and confocal (Fig. 2D) images of a tongue biopsy with the confocal image plane oriented perpendicular to the epithelial surface. Again, the confocal image shows epithelial nuclei throughout the epithelium; tissue architecture and cell morphology assessed by reflectance confocal microscopy compare well to that assessed by histology.

In clinical applications, reflectance confocal images would be obtained with the image plane parallel to the epithelial surface. Figure 3 shows reflectance confocal images obtained in this orientation at different depths beneath the surface of the epithelium. The confocal image from the superficial epithelium (Fig. 3B) shows larger cells with condensed nuclei, while the confocal image obtained 50 microns beneath the epithelial surface (Fig. 3C) shows uniform, smaller intermediate epithelial cells. The confocal image of the basal epithelium (Fig. 3D) shows a distinct increase in cell density and nuclear to cytoplasmic ratio. Confocal image features compare well with the corresponding transverse histologic section (Fig. 3A). This pattern of confocal images was typical of those recorded from normal biopsies in this study.

In contrast, Figs. 4-8 show images that illustrate the features of SCCs with confocal microscopy. Figure 4 shows histologic (Fig. 4A, B) and confocal images (Fig. 4C) of a moderately differentiated SCC from the lateral surface of the tongue. Extensive

variations in cell size, nuclear size and nuclear morphology are resolved in both the histologic section (Fig 4B) and a confocal image taken 100 microns below the epithelial surface (Fig. 4C). Epithelial nuclei (single arrows) appear as bright areas on the confocal image, whereas areas of stroma with inflammation (double arrows) appear dark in the confocal image. Similarly, the histologic (Fig. 5 A, B, D) and confocal images (Fig. 5 C, E) of invasive SCC of the soft palate show regions of tumor cells (single arrows) and interspersed regions of stroma containing inflammatory cells (double arrows). Confocal images obtained 100 microns beneath the epithelial surface show strong backscattering from tumor cell nuclei and dark regions corresponding to areas of inflammation. Nuclear density as assessed by confocal microscopy in the SCCs of Figs. 4 and 5 is clearly higher than in the normal tissue displayed in Fig. 3.

Figure 6 shows histologic and confocal images from a moderately differentiated SCC from the buccal mucosa. Increased keratinization in tumor cells are noted in histologic (Fig. 6B) and confocal images (Fig. 6C) as higher signal return from cytoplasmic, nonnuclear areas (single arrows). Large, homogeneous keratin pearls (Figs. 6D, E) were visible in confocal images as areas of high return with a speckled appearance (single arrows). These features were also observed in images of a well differentiated SCC from the gingiva (Fig. 7). The confocal images show both keratin pearls (double arrows) (Fig. 7C) and tumor cells (single arrows) surrounded by smaller keratin pearls (Fig. 7E). Confocal image features compare well with corresponding histologic images.

In addition to tumor cells and keratin, confocal imaging identified other features in normal and neoplastic oral tissues. Figure 8 shows images from a moderately differentiated SCC from the lateral surface of the tongue. Figures 8B and C show

histologic and confocal images of muscle fibers (single arrows); the muscle fibers do not strongly scatter light and appear dark in the confocal image. Areas of fibrosis in the tumor are clearly discernible in histologic (Fig. 8D) and confocal images (Fig. 8E). Confocal images of fibrosis show scattering from individual fibers (double arrows) as well as elongated fibroblast nuclei (single arrows). Figure 9 shows images from salivary glands (single arrows) in a biopsy specimen from the floor of the mouth. Confocal images of these glands are characterized by bright return from serous demilunes containing serous secreting cells surrounding darker regions of low return from mucous-secreting units[27].

An important performance measure for confocal imaging *in vivo* is the maximum depth at which images can be obtained, or "penetration depth." We observed a wide variation in penetration depth throughout this study. We analyzed image stacks from 13 normal samples in which confocal images throughout the epithelium were captured, and we were able to image up to the confocal microscope's working distance (250 microns) 31% of the time. In 46% of the cases, penetration depth was between 150 – 200 microns, while 23% of the time, penetration depth was 100 – 150 microns. We hypothesize that increased levels of keratin, particularly in the superficial epithelium, can limit the ability of illumination light to penetrate to lower depths due to the high refractive index of keratin compared to cytoplasm ($n_{keratin} = 1.54$[28] versus $n_{cytoplasm} = 1.37$[29]).

Discussion

The confocal images presented here illustrate the ability of reflectance confocal microscopy to image oral mucosa with resolution comparable to histologic evaluation without tissue preparation and staining. In normal tissue, depth-related changes in cell

diameter and nuclear density were observed at multiple anatomic sites within the oral cavity. In SCCs, densely packed, pleomorphic tumor nuclei could be visualized with distinct differences in nuclear density and morphology distinguishable between confocal images of neoplastic and non-neoplastic oral cavity. Other features of non-cancerous and cancerous oral tissue that could be identified in the confocal images included areas of inflammation, fibrosis, muscle fibers and salivary glands. Areas of inflammation appear dark in confocal images of the oral cavity.

The images reported here show similar features in the oral cavity to those reported by White *etal.*[4]. In that study, images of the superficial epithelial layers of the lip and anterior tongue were acquired at depths of up to 490 μm and 250 μm, respectively. Cell nuclei and membranes were clearly resolved in the epithelial layers, correlating well with histology. The use of a low power objective (30X) allowed the capture of different structures in the lamina propria including collagen fibers and blood vessels. The study presented here provides a more comprehensive survey of the morphologic features that can be measured using reflectance confocal microscopy from oral sites such as the floor of the mouth, gingiva, buccal mucosa, soft palate and lateral surfaces of the tongue, and how these features change with the development of SCC.

Confocal microscopy can provide images of many important cellular and architectural features of SCC. While the images presented here were obtained from biopsies measured immediately after excision, we have recently described a fiber optic reflectance confocal microscope that has been used to obtain images of the oral cavity in vivo[7, 8]. This flexible confocal microendoscope is small enough that it can be used to examine sites throughout the oral cavity. The tip of the endoscope is placed in contact

with the tissue to be imaged. A small drop of saline provides index matching between the tip of the endoscope and the tissue. Weak suction is applied at the distal tip of the microendoscope to pull the tissue up through the image plane of the confocal microscope, to easily obtain images at different depths beneath the surface of the epithelium.

The ability to obtain such images *in vivo* and at near real time suggests several potential clinical applications for reflectance confocal microscopy such as noninvasive diagnosis of oral lesions and the ability to determine tumor margins *in vivo* in real time. Visual inspection and palpation remain the standard methods used to assess the extent of mucosal involvement by carcinomas and premalignant lesions. However, molecular and pathologic assessments of "normal appearing" mucosa have revealed molecular and cellular changes in these tissues, illustrating the fallibility of visual detection of dysplasia even by highly trained clinicians[30, 31]. To compensate for the limitation of surgeons to determine exactly the margins of carcinoma or dysplasia, it is accepted practice to resect a large cuff (approximately 1-2 cm.) of normal appearing mucosa around the visibly abnormal tissue. This produces better likelihood of complete excision, but increased postoperative morbidity due to the greater amount of tissue removed. In tertiary care centers, problems caused by the inability to visually distinguish the margins of carcinoma and dysplasia is ameliorated by the use of frozen section to analyze edges of the resection using light microscopy. However, accurate frozen section analysis is time consuming, costly, dependent on the experience and skill of the histotechnician and pathologist, and not available in unspecialized medical facilities. Thus, technological advancements such as *in vivo* confocal imaging that improve the ability of surgeons to accurately identify tumor margins in real time could have substantial benefit for patients. As our results

demonstrate, *in vivo* confocal imaging has the potential to assess features of normal mucosa and SCC, and may yield a very attractive alternative method to assess the status of mucosal margins, through its capability to visualize cellular morphology, and tissue architecture in real time without the need for sectioning and staining. Significant time and cost savings through the use of confocal examination of frozen sections from Mohs micrographic surgery for excision of nonmelanoma skin cancers have already been noted by Rajadhyaksha *etal.*[32]. We acknowledge that a limitation of *in vivo* confocal microscopy is penetration depth and therefore its inability to assess the deep margin of a large, invasive tumor. In addition, verrucous lesions with extreme hyperkeratosis may not permit adequate light penetration to visualize the epithelial stromal border.

Achieving the clinical potential of *in vivo* confocal imaging will require further characterization of the cellular and architectural features of oral tissue that are visible with confocal microscopy and assessment of how they match standard histologic examination. This includes imaging of more dysplastic lesions and the evaluation of the efficiency of confocal imaging in the clinical assessment of margin involvement and response to treatment. Two primary challenges must be addressed in these studies. The first is to obtain images *in vivo* and assess their image characteristics in comparison to our previous results and standard histologic examination; we have just commenced an *in vivo* pilot study of fiber optic reflectance confocal microscopy of oral lesions. The second is to explore methods that can increase the penetration depth at which good quality confocal images can be obtained. We are studying methods to increase penetration depth through the use of additional signal filtering techniques such as coherence gating to better isolate backscattered light from our focal plane[33] and chemical agents such as glucose and glycerol to improve index matching at the surface[4, 34].

In this study, we have shown the power of reflectance confocal microscopy to visualize, at the subcellular level, features of both normal and neoplastic oral mucosa throughout the oral cavity as well as the composition of SCCs with varying differentiation levels. Our results support the potential for this tool to play a significant role in the clinical evaluation of oral lesions, real-time identification of tumor margins, and monitoring of response to therapeutic treatment.

Acknowledgements

We would like to thank Dr. Jon Schwartz from the Department of Molecular Pathology at the University of Texas M. D. Anderson Cancer Center for allowing us to use his brightfield microscope and CCD camera to capture images of histology sections.

The views expressed in this article are those of the author and do not reflect the official policy or position of the United States Air Force, Department of Defense, or the U.S. Government.

References

1. Rajadhyaksha, M., Gonzalez, S., Zavislan, J. M., Anderson, R. R., and Webb, R. H. *In vivo* confocal scanning laser microscopy of human skin II: Advances in instrumentation and comparison with histology. Journal of Investigative Dermatology, *113:* 293-303, 1999.

2. Rajadhyaksha, M., Grossman, M., Esterowitz, D., Webb, R. H., and Anderson, R. R. *In vivo* confocal scanning laser microscopy of human skin: Melanin provides strong contrast. Journal of Investigative Dermatology, *104:* 946-952, 1995.

3. Rajadhyaksha, M., Anderson, R. R., and Webb, R. H. Video-rate confocal scanning laser microscope for imaging human tissues *in vivo*. Applied Optics, *38:* 2105-2115, 1999.

4. White, W. M., Rajadhyaksha, M., Gonzalez, S., Fabian, R. L., and Anderson, R. R. Noninvasive imaging of human oral mucosa *in vivo* by confocal reflectance microscopy. Laryngoscope, *109:* 1709-1717, 1999.

5. Collier, T., Lacy, A., Richards-Kortum, R., Malpica, A., and Follen, M. Near real-time confocal microscopy of amelanotic tissue: Detection of dysplasia in *ex vivo* cervical tissue. Academic Radiology, *9:* 504-512, 2002.

6. Collier, T., Shen, P., de Pradier, B., and Richards-Kortum, R. Near real time confocal microscopy of amelanotic tissue: Dynamics of aceto-whitening enable nuclear segmentation. Optics Express, *6:* 40-48, 2000.

7. Sung, K. B., Liang, C., Descour, M., Collier, T., Follen, M., Malpica, A., and Richards-Kortum, R. Near real time *in vivo* fibre optic confocal microscopy: Sub-cellular structure resolved. Journal of microscopy, *207(Pt) 2:* 137-145, 2002.

8. Sung, K.-B., Chen, L., Descour, M., Collier, T., Follen, M., and Richards-Kortum, R. Fiber-optic confocal reflectance microscope with miniature objective for *in vivo* imaging of human tissues. IEEE Transactions on Biomedical Engineering, *49:* 1168-1172, 2002.

9. Delaney, P. M., Harris, M. R., and King, R. G. A fibre optic bundle confocal endomicroscope. Clinical and Experimental Pharmacology and Physiology, *20:* 197-198, 1993.

10. Tearney, G. J., Webb, R. H., and Bouma, B. E. Spectrally encoded confocal microscopy. Optics Letters, *23:* 1152-1154, 1998.

11. Gmitro, A. F. and Aziz, D. J. Confocal microscopy through a fiber-optic imaging bundle. Optics Letters, *18:* 565-567, 1993.

12. Delaney, P. M., Harris, M. R., and King, R. G. Fiber optic laser scanning confocal microscopy suitable for fluorescence imaging. Applied Optics, *33:* 573-577, 1994.

13. Sabharwal, Y. S., Rouse, A. R., Donaldson, L., Hopkins, M. F., and Gmitro, A. F. Slit-scanning confocal microendoscope for high-resolution *in vivo* imaging. Applied Optics, *38:* 7133-7144, 1999.

14. Knittel, J., Schnieder, L., Guess, G., Messerschmidt, B., and Possner, T. Endoscope-compatible confocal microscope using a gradient index-lens system. Optics Communications, *188:* 267-273, 2001.

15. Lane, P., Dlugan, A., and MacAulay, C. DMD enabled confocal microendoscopy. *In:* Coherence Domain Methods in Biomedical Science and Clinical Applications V, San Jose, CA, 2001, pp. 192-1998.

16. Bertrand, C. and Corcuff, P. *In vivo* spatio-temporal visualization of the human skin by real-time confocal microscopy. Scanning, *16:* 150-154, 1993.

17. Corcuff, P., Gonnord, G., Piérard, G. E., and Lévéque, J. L. *In vivo* confocal microscopy of human skin: A new design for cosmetology and dermatology. Scanning, *18:* 351-355, 1996.

18. Masters, B. R., Aziz, D. J., Gmitro, A. F., Kerr, J. H., O'Grady, T. C., and Goldman, L. Rapid observation of unfixed, unstained human skin biopsy specimens with confocal microscopy and visualization. Journal of Biomedical Optics, *2:* 437-445, 1997.

19. González, S., Rajadhyaksha, M., Rubinstein, G., and Anderson, R. R. Characterization of psoriasis *in vivo* by reflectance confocal microscopy. Journal of medicine, *30:* 337-356, 1999.

20. Gonzalez, S., Rajadhyaksha, M., Gonzalez-Serva, A., White, W. M., and Anderson, R. R. Confocal reflectance imaging of folliculitis *in vivo*: Correlation with routine histology. Journal of Cutaneous Pathology, *26:* 201-205, 1999.

21. Busam, K. J., Hester, K., Charles, C., Sachs, D. L., Antonescu, C. R., Gonzalez, S., and Halpern, A. C. Detection of clinically amelanotic malignant melanoma and assessment of its margins by *in vivo* confocal scanning laser microscopy. Archives of dermatology, *137:* 923-929, 2001.

22. Langley, R. G., Rajadhyaksha, M., Dwyer, P. J., Sober, A. J., Flotte, T. J., and Anderson, R. R. Confocal scanning laser microscopy of benign and malignant melanocytic skin lesions *in vivo*. Journal of the American Academy of Dermatology, *45:* 365-376, 2001.

23. Gonzalez, S. and Tannous, Z. Real-time, *in vivo* confocal reflectance microscopy of basal cell carcinoma. Journal of the American Academy of Dermatology, *47:* 869-874, 2002.

24. Inoue, H., Igari, T., Nishikage, T., Ami, K., Yoshida, T., and Iwai, T. A novel method of virtual histopathology using laser-scanning confocal microscopy in-vitro with untreated fresh specimens from the gastrointestinal mucosa. Endoscopy, *32:* 439-443, 2000.

25. Drezek, R. A., Collier, T., Brookner, C. K., Malpica, A., Lotan, R., Richards-Kortum, R. R., and Follen, M. Laser scanning confocal microscopy of cervical

tissue before and after application of acetic acid. American journal of obstetrics and gynecology, *182:* 1135-1139, 2000.

26. Smithpeter, C. L., Dunn, A. K., Welch, A. J., and Richards-Kortum, R. Penetration depth limits of *in vivo* confocal reflectance imaging. Applied Optics, *37:* 2749-2754, 1998.

27. Riviere, H. L. Lab Manual of Normal Oral Histology. Chicago, IL: Quintessence Publishing Co., Inc, 2000.

28. Prum, R. O., Torres, R. H., Williamson, S., and Dyck, J. Coherent light scattering by blue feather barbs. Nature, *396:* 28-29, 1998.

29. Brunsting, A. and Mullaney, P. F. Differential light scattering from spherical mammalian cells. Biophysical Journal, *14:* 439-453, 1974.

30. Incze, J., Vaughan, C. W., Jr., Lui, P., Strong, M. S., and Kulapaditharom, B. Premalignant changes in normal appearing epithelium in patients with squamous cell carcinoma of the upper aerodigestive tract. American journal of surgery, *144:* 401-405, 1982.

31. Brennan, J. A. and Sidransky, D. Molecular staging of head and neck squamous carcinoma. Cancer and metastasis reviews, *15:* 3-10, 1996.

32. Rajadhyaksha, M., Menaker, G., Flotte, T., Dwyer, P. J., and González, S. Confocal examination of nonmelanoma cancers in thick skin excisions to potentially guide Mohs micrographic surgery without frozen histopathology. The Journal of investigative dermatology, *117:* 1137-1143, 2001.

33. Izatt, J. A., Kulkarni, M. D., Wang, H.-W., Kobayashi, K., and Sivak, M. V. Optical coherence tomography and microscopy in gastrointestinal tissues. IEEE Journal of Selected Topics in Quantum Electronics, *2:* 1017-1028, 1996.

34. Vargas, G., Chan, K. F., Thomsen, S. L., and Welch, A. J. Use of osmotically active agents to alter optical properties of tissue: Effects on the detected fluorescence signal measured through skin. Lasers in surgery and medicine, *29:* 213-220, 2001.

Table 1. Number of clinically normal and abnormal biopsies from each site.

Location	**Clinical Appearance**	
	Normal	**Abnormal**
Tongue (Lateral and Ventral Surfaces)	8	8
Floor of Mouth	2	2
Gingiva	2	3
Buccal Mucosa	2	1
Soft Palate	1	1

Table 2. Histopathologic diagnosis by patient.

Pat.	Site	Histopathologic Diagnosis	
		Clinically Normal Biopsy	**Clinically Abnormal Biopsy**
1	Tongue (lateral surface)	Hyperkeratosis	Moderately differentiated SCC
2	Buccal mucosa	Hyperkeratosis	Moderately differentiated SCC
3	Floor of mouth	Mild hyperkeratosis	Hyperkeratosis, hyperplasia
4	Tongue (lateral surface)	Mild hyperplasia	Moderately differentiated SCC
5	Tongue (ventral surface)	Hyperkeratosis	Extreme hyperkeratosis
6	Tongue (lateral surface)	Mild hyperplasia	Moderately differentiated SCC
7	Gingiva	None[1]	Well differentiated SCC
8	Gingiva	Mild hyperkeratosis	Moderately differentiated SCC
9	Tongue (lateral surface)	Hyperkeratosis	Moderately differentiated SCC
10	Tongue (ventral surface)	Hyperkeratosis	None[1]
11	Tongue (lateral surface)	Hyperkeratosis, hyperplasia	None[1]
12	Floor of mouth	Hyperkeratosis, hyperplasia	Moderately differentiated SCC
13	Tongue (lateral surface)	Parakeratosis, hyperplasia	Moderately differentiated SCC
14	Soft Palate	Hyperkeratosis	Moderately differentiated SCC
15	Gingiva	Hyperkeratosis	Mild hyperkeratotic dysplasia

[1]No epithelium in specimen.

Fig. 1 Block diagram of the near real-time reflectance confocal microscope used to image oral cavity specimens.

Fig. 2 Comparison of confocal images to histologic sections. The histology section (A) and mosaic of confocal images (B) from a 200 micron thick transverse organ culture of a normal gingiva biopsy show epithelium and stroma; the basal epithelial nuclei are readily apparent at the epithelial stromal junction (double arrows). Epithelial cell nuclei and fibroblast nuclei (single arrow) are resolved. The histology section (C) and transverse confocal image (D) of a hyperkeratotic tongue biopsy show epithelial cell nuclei from superficial epithelium on the right (double arrows) to the basal layer (single arrow) on the left. Scale bars = 50 microns.

Fig. 3 Transverse histologic image (A) and en face confocal images (B-D) obtained at different depths beneath the epithelial surface from hyperkeratotic tissue from the ventral tongue surface. Nuclear density, cell size, and cytoplasmic scattering change as the depth of the focal plane increases from (B) 20 microns to (C) 50 microns to (D) 150 microns beneath the epithelial surface. Scale bars = 50 microns.

Fig. 4 Histologic and confocal images of a moderately differentiated SCC from the lateral surface of the tongue. (A) Low magnification image of a keratin antibody (MMAC) stained section showing tumor cells interspersed with stroma containing inflammation (2.5X objective). (B) High magnification image of tumor cells (single arrows) containing pleomorphic nuclei and stroma with inflammation (double arrows).

(C) Confocal image taken 100 microns below the epithelial surface illustrating pleomorphic nuclei (single arrows) and dark areas corresponding to stroma containing inflammation (double arrows). Scale bars = 50 microns.

Fig. 5 Confocal and histologic mages of invasive SCC of the soft palate. **(A)** Low magnification image of a keratin antibody (MMAC) stained section showing extensive tumor cells surrounding areas of stroma with inflammation (2.5X objective). **(B)** High magnification image of keratinized, tightly packed tumor cells (single arrow) with stroma containing inflammation (double arrows) (20X objective). **(C)** Confocal image taken 100 microns below the surface of tightly packed, highly scattering tumor cells (single arrow) with dark areas of stroma with inflammation (double arrows). **(D)** High magnification histologic image of less keratinized, larger tumor cells (single arrow) with stroma containing inflammation (double arrows) (20X objective). **(E)** Confocal image taken 100 microns below the surface with larger cells (single arrow) and less background scattering combined with dark areas of stroma with inflammation (double arrows). Scale bars = 50 microns.

Fig. 6 Images of a moderately differentiated SCC from the buccal mucosa. (A) Low magnification image of a keratin antibody (MMAC) stained section showing keratin pearls, highly keratinized tumor cells, and stroma with inflammation (2.5X objective). (B) High magnification histologic image of tumor cells (single arrow) and stroma containing inflammation (double arrows) (20X objective). (C) Confocal image taken 200 microns below the epithelial surface showing dark regions of stroma with inflammation

(double arrows) alternating with tightly packed tumor cells (single arrow) containing irregular nuclei. (D) High magnification histologic image of a keratin pearl (single arrow) (20X objective). (E) Confocal image of a keratin pearl (single arrow) taken 50 microns below the surface showing the highly reflective, speckled appearance characteristic of keratin. Scale bars = 50 microns.

Fig. 7 Images of a well differentiated SCC from the gingiva. (A) Low magnification image of a keratin antibody (MMAC) stained section showing tumor cells and keratin pearls interspersed with stroma containing inflammation (2.5X objective). (B) High magnification histologic image of a keratin pearl (double arrows) (20X objective). (C) Confocal image taken 50 microns below the surface containing highly reflective keratin (double arrows). (D) High magnification histologic image of keratin pearls with highly keratinized tumor cells (single arrow) (20X objective). (E) Confocal image taken 50 microns below the surface containing areas of highly reflective keratin with nuclei (single arrow). Scale bars = 50 microns.

Fig. 8 Images of a muscle and fibrosis from a moderately differentiated SCC from the lateral surface of the tongue. (A) Low magnification image of an H&E section show skeletal muscle and extensive fibrosis (2.5X objective). (B) High magnification histologic image of muscle (single arrow) (20X objective). (C) Confocal image of muscle (single arrow) taken 100 microns below the surface. (D) High magnification histologic image of fibrosis (double arrows) with elongated fibroblast nuclei (single arrow) (20X objective). (E) Confocal image of fibrosis (double arrows) taken 50 microns

below the surface illustrating reflectance from structural protein fibers and containing elongated fibroblast nuclei (single arrow). Scale bars = 50 microns.

Fig. 9 Images of salivary glands from the floor of the mouth. (A) Low magnification image of a keratin antibody (MMAC) stained section showing extensive salivary glands (2.5X objective). (B) High magnification histologic image of salivary glands (single arrow) (20X objective). (C) Confocal image of salivary glands (single arrow) taken 50 microns below the surface. Scale bars = 50 microns.

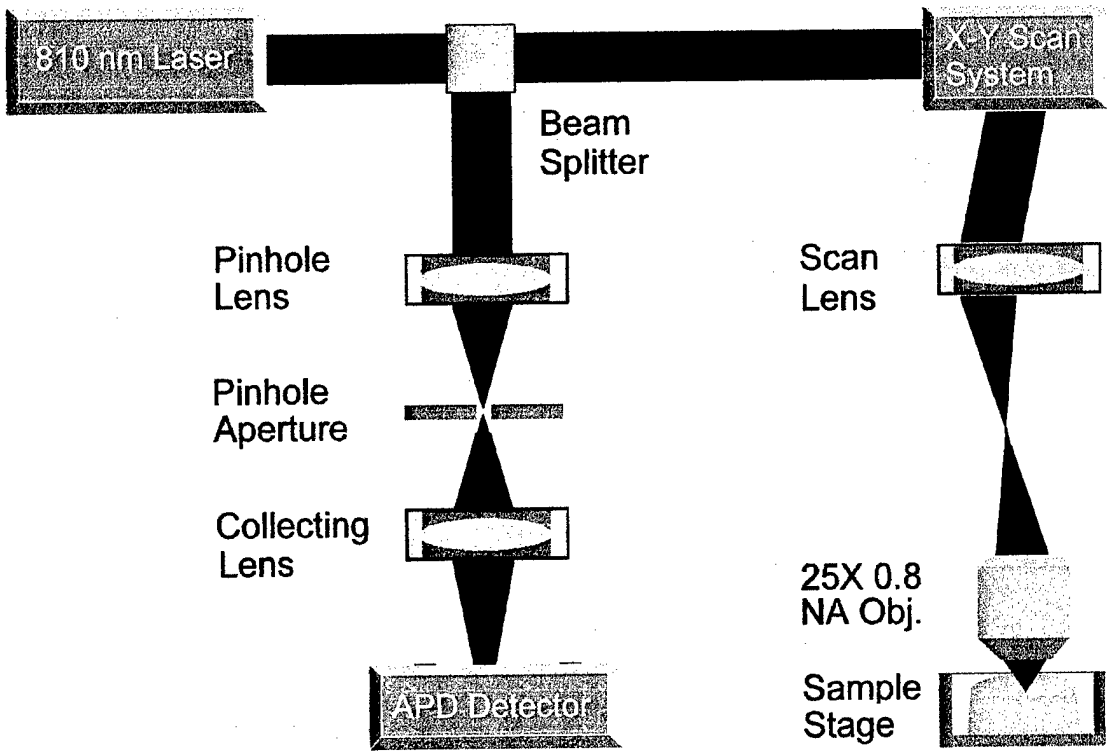
810 nm Laser
X-Y Scan System
Beam Splitter
Pinhole Lens
Scan Lens
Pinhole Aperture
Collecting Lens
25X 0.8 NA Obj.
APD Detector
Sample Stage

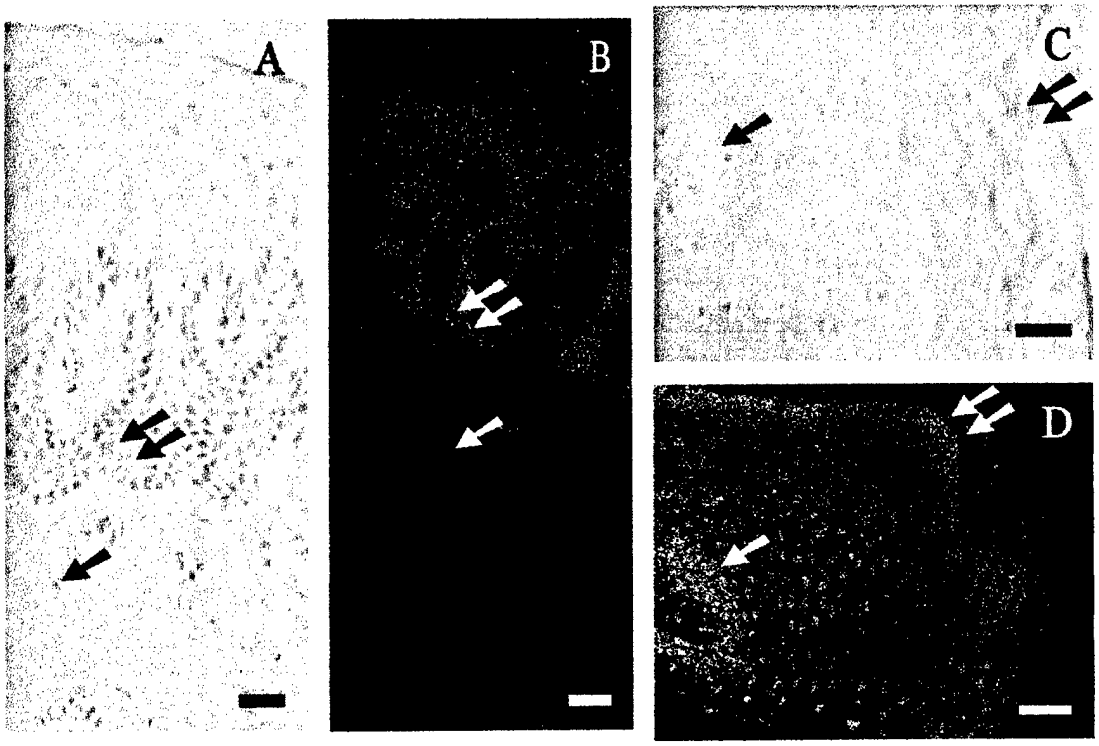
A
B
C
D

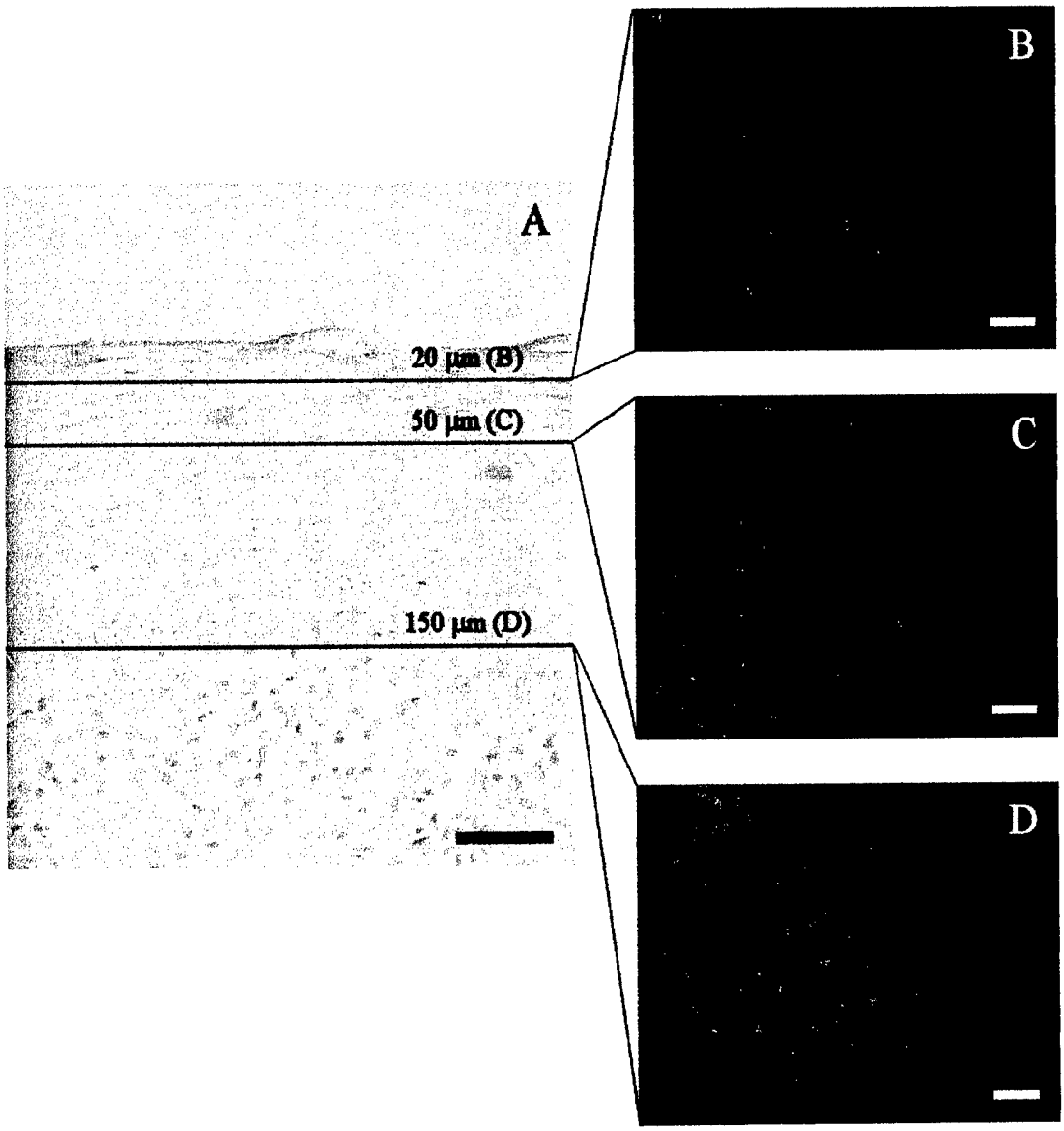
A
B
C
D
20 µm (B)
50 µm (C)
150 µm (D)


A
B
C

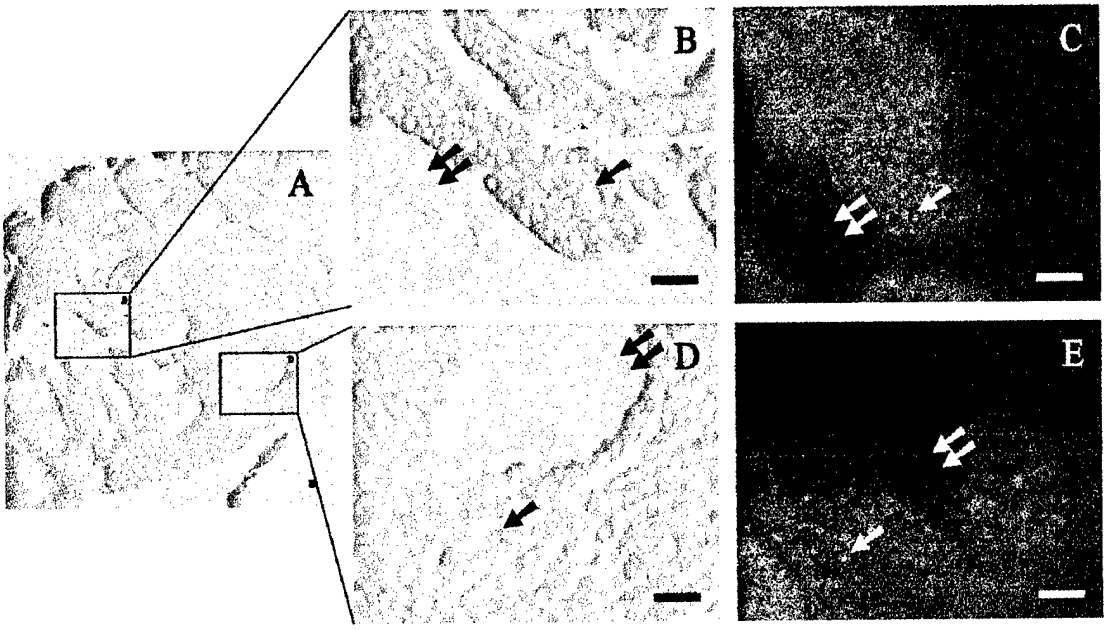
A
B
C
D
E

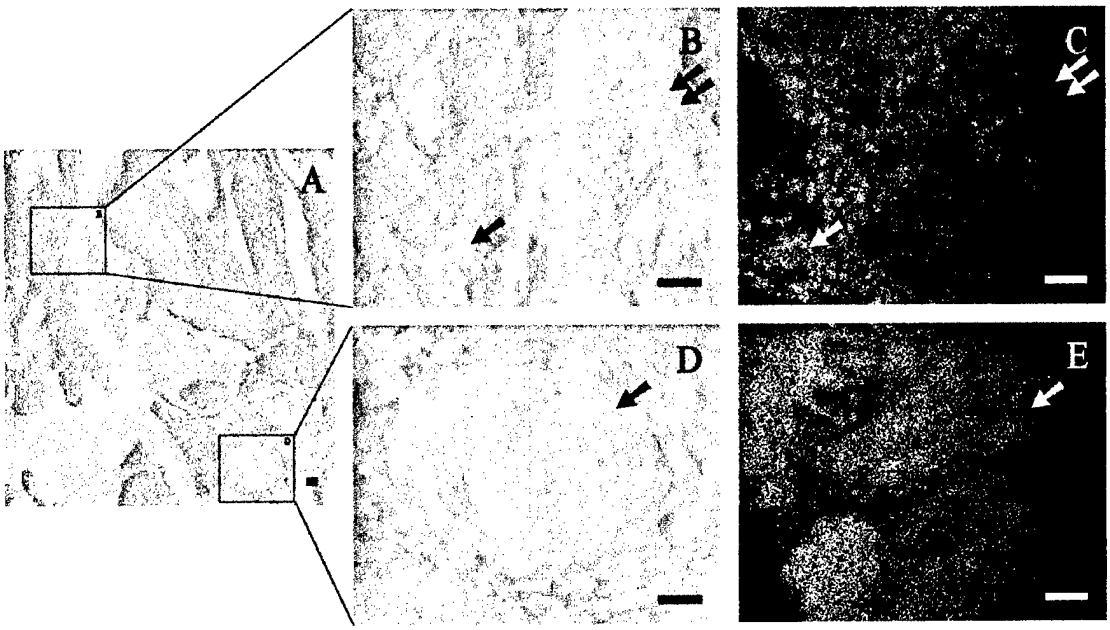
A
B
C
D
E

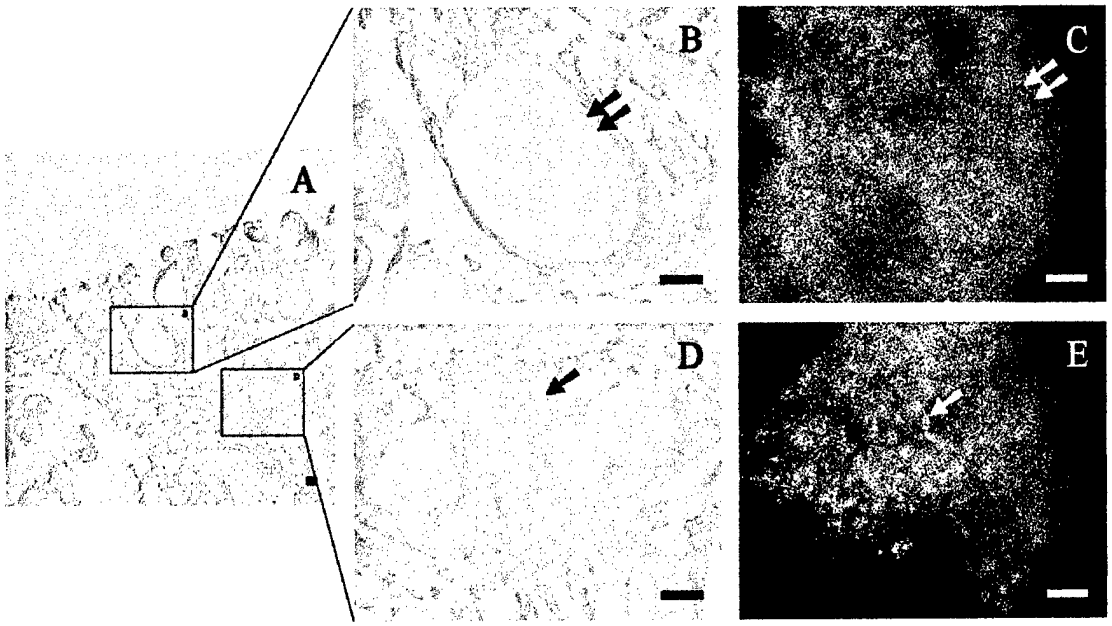
A
B
C
D
E

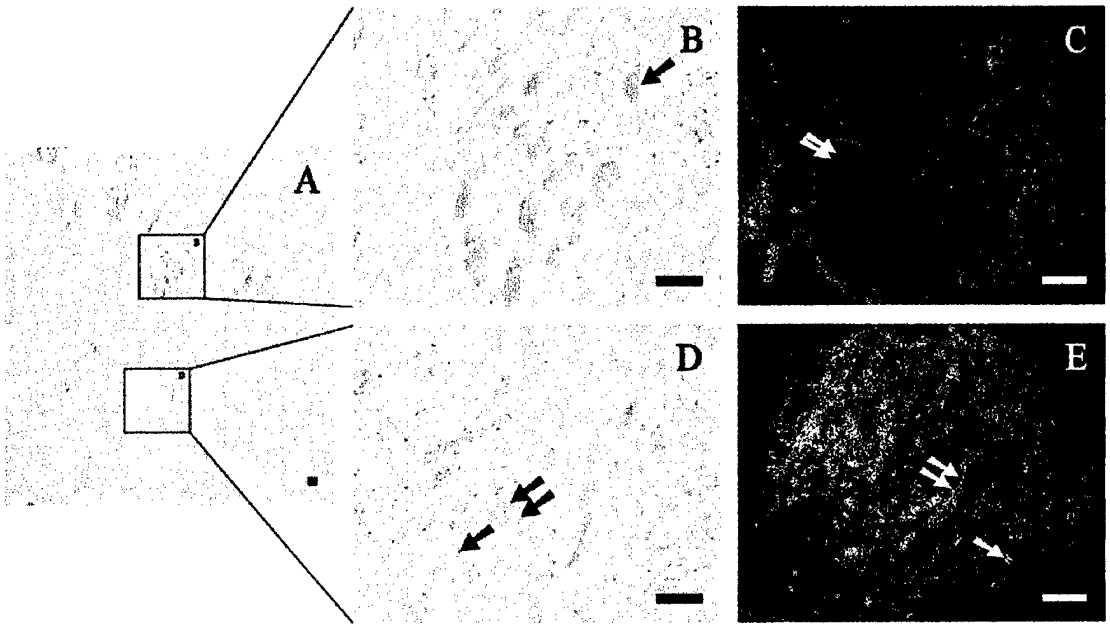
A
B
C
D
E

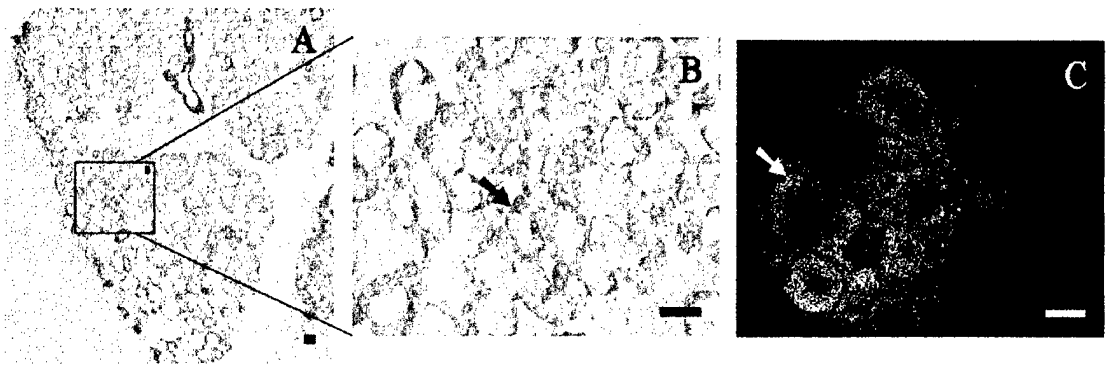
A
B
C